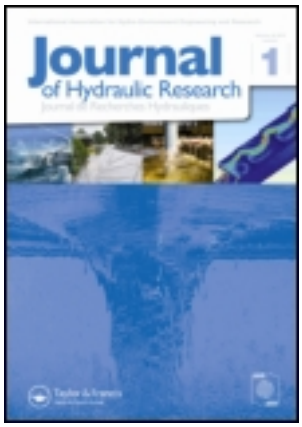

Journal of Hydraulic Research
Publication details, including instructions for authors and subscription information:
http://www.tandfonline.com/loi/tjhr20

Propagation of surge waves in channels with large-scale bank roughness

Tobias Meile [a] , Jean-Louis Boillat [b] & Anton J. Schleiss [c]

[a] Laboratory of Hydraulic Constructions (LCH), Institute of Civil Engineering, Ecole polytechnique fédérale de Lausanne (EPFL), Station 18, CH-1015 Lausanne, Switzerland (now at Basler & Hofmann West AG, Industriestrasse 1, CH-3052 Zollikofen, Switzerland) E-mail:

[b] Laboratory of Hydraulic Constructions (LCH), Institute of Civil Engineering, Ecole polytechnique fédérale de Lausanne (EPFL), Station 18, CH-1015, Lausanne, Switzerland E-mail:

[c] Laboratory of Hydraulic Constructions (LCH), Institute of Civil Engineering, Ecole polytechnique fédérale de Lausanne (EPFL), Station 18, CH-1015, Lausanne, Switzerland
Version of record first published: 08 Mar 2013.

To cite this article: Tobias Meile , Jean-Louis Boillat & Anton J. Schleiss (2013): Propagation of surge waves in channels with large-scale bank roughness, Journal of Hydraulic Research, 51:2, 195-202

To link to this article: http://dx.doi.org/10.1080/00221686.2012.738876

Journal of Hydraulic Research Vol. 51, No. 2 (2013), pp. 195–202
http://dx.doi.org/10.1080/00221686.2012.738876

Research paper

Propagation of surge waves in channels with large-scale bank roughness

TOBIAS MEILE, Research Assistant, *Laboratory of Hydraulic Constructions (LCH), Institute of Civil Engineering, Ecole polytechnique fédérale de Lausanne (EPFL), Station 18, CH-1015 Lausanne, Switzerland (now at Basler & Hofmann West AG, Industriestrasse 1, CH-3052 Zollikofen, Switzerland).*
Email: tobias.meile@baslerhofmann.ch

JEAN-LOUIS BOILLAT, Senior Research Associate, *Laboratory of Hydraulic Constructions (LCH), Institute of Civil Engineering, Ecole polytechnique fédérale de Lausanne (EPFL), Station 18, CH-1015 Lausanne, Switzerland.*
Email: jean-louis.boillat@epfl.ch

ANTON J. SCHLEISS (IAHR Member), Professor, *Laboratory of Hydraulic Constructions (LCH), Institute of Civil Engineering, Ecole polytechnique fédérale de Lausanne (EPFL), Station 18, CH-1015 Lausanne, Switzerland.*
Email: anton.schleiss@epfl.ch (author for correspondence)

ABSTRACT
Surge waves from upstream have been studied systematically in a 40 m long channel. Its banks were equipped with large-scale rectangular roughness elements. In addition to a prismatic reference channel, 41 different configurations of rectangular bank cavities have been investigated. The purpose was to study the effect of large-scale bank roughness on steady and unsteady flows. The macro-roughness of the channel banks increases the flow resistance. Consequently, the absolute celerity of the surge wave front is also reduced by between 5 and 25%. Based on the concept of an effective channel width for the computation of the mean flow velocity, the relative celerity of the surge wave can be predicted for macro-rough channel configurations. The attenuation of the wave front height is increased by the macro-rough flow resistance as well as by the partial reflections of the surge waves in the cavities and passive retention of the latter.

Keywords: Flow resistance; hydraulic model; macro-roughness; surge wave experiment; unsteady channel flow

1 Introduction

The influence of macro-roughness elements along channel banks during unsteady flow conditions due to surge waves was systematically studied (Meile 2007). Together with the prismatic channel reference, 41 configurations of macro-rough banks and various discharges were tested in a 40 m long flume of 0.114% bed slope. A special experimental set-up was designed able to generate surge waves characterized by different discharge ratios. The first step of the experimentation focused on the determination of the flow resistance under steady flow conditions caused by large-scale roughness elements of the channel banks, namely rectangular cavities. The detailed results and the analysis of the steady flow tests have been published by Meile *et al*. (2011) and are not discussed herein. In a second step, surge waves, induced at the channel entrance, were tested for the same geometries, considering five different discharge scenarios for each geometry.

The practical motivation for this fundamental research was to understand how morphological measures for river revitalization, including lateral cavities at the banks and local widening, could mitigate by surge wave attenuation the harmful effects of hydro-peaking. The latter result from the operation of high-head storage hydropower plants, which mainly operate their turbines during periods of high energy demand. The sudden start and shut-down of turbines causes rapidly-varied unsteady flows (Meile *et al*. 2010).

Experiments with rapidly-unsteady flow in the field of open-channel hydraulics mainly cover three domains: first, experiments on dam-break waves due to the sudden failure of a dam (Schoklitsch 1917, Dressler 1954, Lauber and Hager 1998a, 1998b, Leal *et al*. 2006), second experiments dealing with positive and negative surge waves from up- or downstream due to sluice gate or fast turbine operations including a base-flow (Favre 1935) and finally experiments focusing on secondary waves (Favre 1935, Faure and Nahas 1961, Benet and Cunge

Revision received 8 October 2012/Open for discussion until 30 October 2013.

ISSN 0022-1686 print/ISSN 1814-2079 online
http://www.tandfonline.com

1971, Zairov and Listrovoy 1983, Treske 1994, Soares-Frazão and Zech 2002). Since secondary waves were first observed by Favre (1935) they are also called "Favre waves" and occur behind the wave front.

The propagation speed of small positive and negative surge waves travelling from up- and downstream were systematically studied by Bazin (1865). The theoretical and experimental work of Favre (1935) resulted in equations for the determination of the absolute wave celerity and the height of the surge wave front due to a sudden change of discharge. Further tests with surge waves over a downstream base-flow were conducted by Ünsal (1983), and Zairov and Listrovoy (1983).

No experiments were performed in channels equipped with rectangular large-scale macro-roughness elements on channel banks as far as the authors are aware. This work presents the results of systematic tests in these channel geometries, conducted under controlled laboratory conditions with a steady flow downstream of the surge wave front. Besides the description of rapidly-unsteady flow for macro-rough configurations on the channel banks, this work analyses the surge wave front speed as well as the attenuation of the surge wave front height.

2 Definition of surge waves

Unsteady, non-uniform and rapidly-varied flow is characterized by a free surface including sudden changes and high curvatures. As a consequence, the assumption of hydrostatic pressure is not valid on a limited channel reach. A sudden change in the discharge or the water-level can cause a rapidly-varied flow called a surge wave. The four different types of surge waves include (Favre 1935, Chow 1959, Henderson 1966, Graf and Altinakar 1996) the positive surge wave moving downstream or upstream and the negative (surge) wave moving downstream or upstream.

In a horizontal, frictionless rectangular channel of width B and base-flow $Q_1 = U_1 B h_1$, the sudden increase in discharge at the upstream channel border leads to a positive surge with a steep front. The absolute celerity V_w of the surge wave front travelling downstream is derived from the momentum and continuity equation as (Chow 1959)

$$V_w = U_1 + \sqrt{g h_1} \cdot \sqrt{\frac{h_2}{2h_1}\left(1 + \frac{h_2}{h_1}\right)} \qquad (1)$$

where h_1 is the initial flow depth, U_1 the initial flow velocity, h_2 the surge flow depth and g the gravity acceleration (Fig. 1). Neither the height of the surge wave front $h_1' = h_2 - h_1$ nor the propagation speed is modified along the channel considered (Fig. 1a).

If friction and bottom slope are taken into account (Fig. 1b), the height of the surge wave front decreases along the channel and the wave body deforms (Favre 1935, Zairov and Listrovoy 1983). Further, a positive surge with a steep front does not necessarily develop due to an increase in discharge at the upstream channel

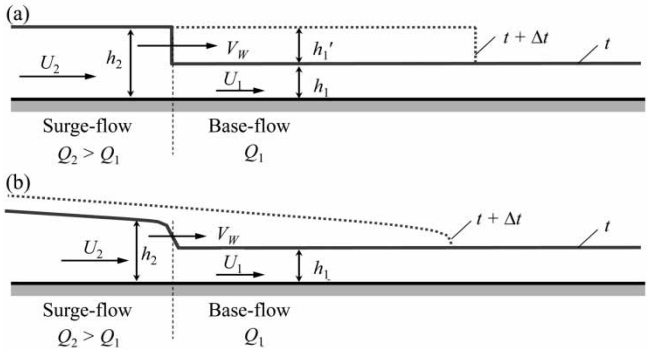

Figure 1 Positive surge from upstream in (a) horizontal, prismatic and frictionless channel, (b) channel including bottom and friction slope

end under the influence of friction and bottom slope. For a wide channel of constant bottom slope with a flow resistance described by Chézy's formula, Henderson (1966) developed a criterion for the formation of a positive surge wave from relatively small disturbances.

3 Experiments

3.1 *Test flume and geometrical configurations*

The hydraulic experiments were performed in a flume 38.33 m long and of 0.114% slope. As shown in Fig. 2, it was divided into a prismatic inlet reach (7.71 m long), a middle reach with large-scale depressions at the banks (26.92 m) and a prismatic outlet reach (4.0 m long). The channel bottom was of painted steel. The sidewalls of the reach with rectangular cavities and the outlet reach were formed by smooth limestone bricks (0.25 m long, 0.10 m wide and 0.19 m high). The equivalent sand roughness of the wall and the painted steel bottom are $k_{sw} = 0.021$ mm and $k_{s_0} = 0.001$ mm, respectively (Meile *et al*. 2011).

The width $B = 0.485 \pm 0.002$ m was used as the prismatic reference channel for all tests. The macro-roughness elements are considered as large-scale depression roughness at both channel banks as described by Morris (1955). They are characterized by the cavity length $L_b = 0.5$, 1.0 or 2.0 m, the cavity spacing $L_c = 0.5, 1.0$ or 2.0 m, and the lateral cavity depth $\Delta B = 0.1, 0.2$, 0.3 or 0.4 m. These geometrical parameters were varied systematically to obtain various aspect and expansion ratios of the cavity defined as $\Delta B/L_b$ and $(B + 2\Delta B)/B$, respectively. The combination of three different values for L_b and L_c and four different

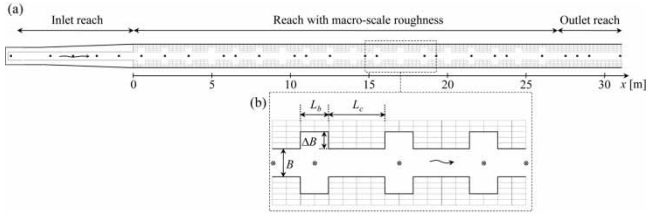

Figure 2 (a) Plan view of test flume, (b) definition of parameters L_b, L_c and ΔB of macro-rough configurations with ⊗ locations of USs

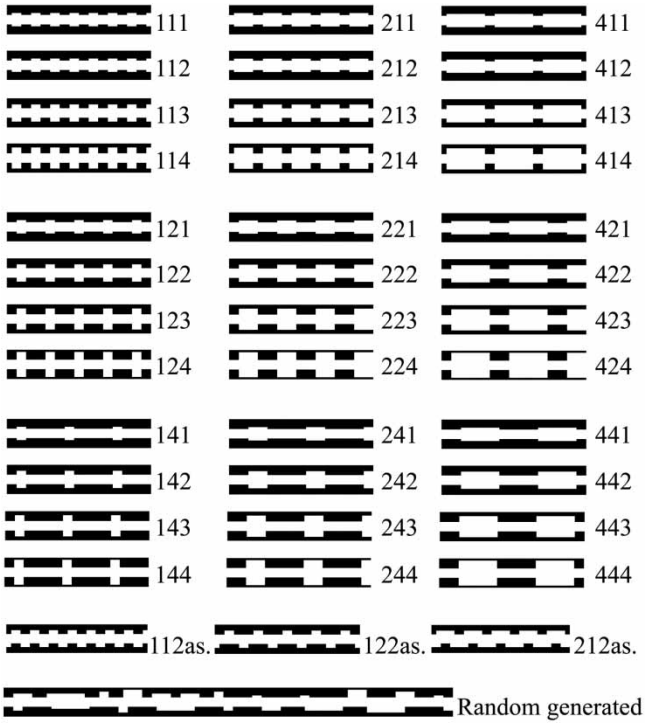

Figure 3 Investigated configurations of macro-roughness of channel banks (Meile *et al*. 2011). Configurations are numbered as follows: first number denotes cavity length L_b ($1 = 0.5$ m, $2 = 1.0$ m, $4 = 2.0$ m), second number denotes distance between cavities L_c ($1 = 0.5$ m, $2 = 1.0$ m, $4 = 2.0$ m); third number denotes lateral cavity depth ΔB ($1 = 0.1$ m, $2 = 0.2$ m, $3 = 0.3$ m; $4 = 0.4$ m)

values of ΔB results in 36 different, axisymmetric geometrical configurations covering eight aspect and four expansion ratios. Additionally, 3 of the 36 axisymmetric configurations have been tested in the asymmetric arrangement and also a randomly-generated configuration was analysed. All configurations tested are shown in Fig. 3.

As mentioned, steady flow tests were conducted in a first step by introducing a steady base discharge at the upstream channel end through a 0.50 m wide and 0.90 m long, horizontal bottom opening of the inlet basin. The purpose was to determine the flow resistance due to macro-rough banks. By separating the observed flow behaviour into a normal recirculating flow, a reattachment and a square-grooved flow type, macro-rough flow resistance formulas were developed using the power-law optimization and a semi-empirical drag coefficient model as described by Meile *et al*. (2011).

3.2 *Measurement equipment and data acquisition*

The water-level raw data (voltage between 0 and 10 V) were recorded with ultrasonic sensors (USs) of 32 Hz sampling rate. The voltage was transformed from a distance to a reference level by calibration of each US to determine the water-level under each US and consequently the flow depth. The data were first filtered by replacing erroneous measurements with the average of neighbour data and then averaged over 0.15625 s. The moving

Figure 4 Setup generating positive and negative surge waves. ① Upper basin, ② water supply pipes and ③ spillway crest placed on ④ experimental flume

average over five values was identified to be the best compromise between a necessary data smoothening and the ability to measure water levels during rapidly-varied unsteady flow.

To measure the propagation and deformation of surge waves, a large number of US were distributed uniformly along the channel (Fig. 2). A 1D-velocity profile using the ultrasonic Doppler shift effect was recorded for selected tests in the channel axis at location $x = 16.92$ m (Fig. 2). These results are discussed by Meile *et al*. (2008).

3.3 *Unsteady flow tests and test procedures*

The experimental facility was designed so that a certain discharge was added rapidly to the well-established base-flow to generate surge waves. An upper basin with a separate water supply system was placed above the inlet basin (Fig. 4). Its water was released by six vertical pipes of different diameters into the inlet basin of the channel. The sudden opening or closure of the flap gates at the bottom of one or several pipe(s) generated the desired surges from upstream. Each geometrical configuration was investigated under 5–30 scenarios of rapidly-varied unsteady flow (Table 1). Compared with dam-break waves, the tested waves are relatively moderate as typical for hydro-peaking conditions in rivers. The ratio $\Delta Q/Q_{mean} = \Delta Q/(Q_b + 0.5\Delta Q)$ is used (Meile *et al*. 2010) as a hydro-peaking indicator; it varied between 0.10 and 1.64.

In the surge Runs 3, 8, 13, 18 and 23 of Table 1 (in bold) all geometrical configurations of bank macro-roughness were systematically tested. All other scenarios were investigated for geometrical configurations with $\Delta B = 0.20$ m and $\Delta B = 0.40$ m only (configurations xx2 and xx4 of Fig. 3). The test procedure for unsteady flow conditions included the following steps:

(a) Regulation of base-flow and inflow to upper basin.
(b) Observation of base-flow until steady flow conditions occurred.

Table 1 Scenarios 1–30 of unsteady flow tests

Scenario	1	2	**3**	4	5	6	7	**8**	9	10	11	12	**13**	14	15
Q_b	6.0	5.9	**6.0**	6.2	5.9	10.7	10.7	**10.7**	10.7	10.7	19.2	19.1	**19.0**	18.9	18.7
Q_{total}	12.5	17.0	**23.6**	36.7	59.4	17.2	21.8	**28.3**	41.1	64.1	25.7	30.2	**36.5**	49.2	71.8
ΔQ	6.5	11.1	**17.6**	30.5	53.5	6.5	11.1	**17.6**	30.4	53.4	6.5	11.1	**17.5**	30.3	53.1
Scenario	16	17	**18**	19	20	21	22	**23**	24	25	26	27	28	29	30
Q_b	34.7	34.8	**34.4**	34.9	35.0	49.1	48.7	**48.8**	48.7	48.6	62.3	61.0	60.8	61.0	60.9
Q_{total}	41.1	45.7	**51.8**	64.9	87.7	55.5	59.6	**66.0**	78.5	100.8	68.6	71.8	77.9	90.6	112.9
ΔQ	6.4	10.9	**17.4**	30.0	52.7	6.4	10.9	**17.2**	29.8	52.2	6.3	10.8	17.1	29.6	52.0

Note: All discharges are given in (l/s).

(c) Determination of discharge (base-flow and inflow to upper basin) by instantaneous values measured by electromagnetic flow meter.
(d) Start of recording water levels by measurement of 11,520 (9600) values corresponding to 6 (4) min at 32 Hz.
(e) Start recording with video camera located laterally at outlet reach.
(f) Opening of flap gates corresponding to a certain scenario after some 30 s of recording.
(g) Observation and documentation of positive surge wave.
(h) Closure of flap gates corresponding to a certain scenario after some 30 s of recording and observation of negative surge wave.

4 Results

4.1 *Wave classification*

In the following a detailed classification of the tested waves is provided for the positive waves from upstream in the prismatic channel configuration. The criterion of Ponce *et al*. (1978) and the classification diagram of Chung and Kang (2006) were applied. Three preliminary steps are necessary to classify the waves:

(a) Verification of shallow water wave hypothesis (Henderson 1966): $\lambda/h > 50$, with λ as wavelength and h as flow depth.
(b) Identification of evolution of wave front along channel regarding its formation and stabilization of the shape.
(c) Estimation of time to peak value t_p as a characteristic unsteady flow parameter.

Shallow water hypothesis: A positive wave is generated by opening, whereas a negative wave is generated by closing of the flap gates of the surge wave set-up. The latter was never produced before the arrival of the positive wave at the channel end. For a length of 38.33 m and a maximum available flow depth of 0.38 m, the relative wavelength is therefore at least $\lambda/h > 101$. Thus, the shallow water wave hypothesis is confirmed.

Evolution of wave front and the time to peak value are simultaneously determined by analysing the steepness of the wave front at different locations along the prismatic reference channel. Three different US were considered. Sensor 0 ($x = -7.71$ m) was located just downstream of the inlet basin, sensors 5 and 13 at $x = 0.42$ and 12.42 m from the end of the inlet reach. The time to peak values t_p determined from the level recordings are presented in Fig. 5 as a function of the surge wave indicator $\Delta Q/Q_{mean}$ for the three different sensors.

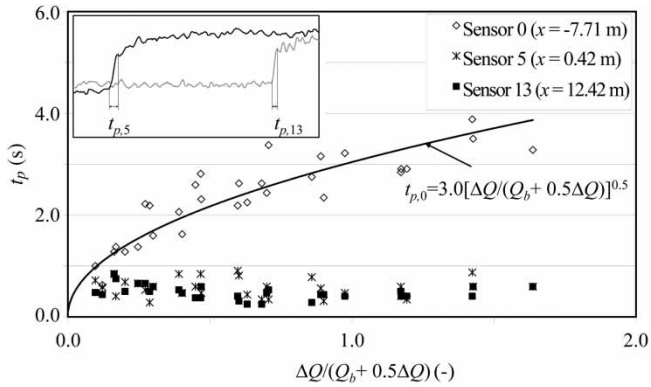

Figure 5 Time to peak values t_p versus $\Delta Q/(Q_b + 0.5\Delta Q)$ at USs 0 ($x = -7.71$ m), 5 ($x = 0.42$ m), 13 ($x = 12.42$ m) for all 30 scenarios of prismatic reference channel

Time to peak value is a function of $3.0[\Delta Q/(Q_b + 0.5\Delta Q)]^{0.5}$ at US0 ($x = -7.71$ m) (Fig. 5). Further downstream at $x = 0.42$ and 12.42 m t_p is almost independent of the discharge wave characteristics. Since the values of t_p at $x = 0.42$ m are slightly below those at $x = 12.42$ m in Fig. 5, the wave slightly steepens along the channel. Nevertheless, a quite stable waveform resulted already after the inlet reach. At the upstream channel end ($x = -7.71$ m) t_p was about 1–10 times higher. At US0, they are consequently influenced by the inertia of the wave generating set-up, whereas the time to peak values at locations $x = 0.42$ and 12.42 m are smaller due to the overrun phenomenon. However, the opening time and the inertia of the surge wave generation set-up were small enough to obtain a positive wave with a steep front (e.g. Fig. 7 for $x = -7.71$ m). After a short channel reach, the wave characteristics became independent of the flap gate opening time, in agreement with Favre (1935). This indicates that operation times of up to 6 s do not influence the shape of the surge formed.

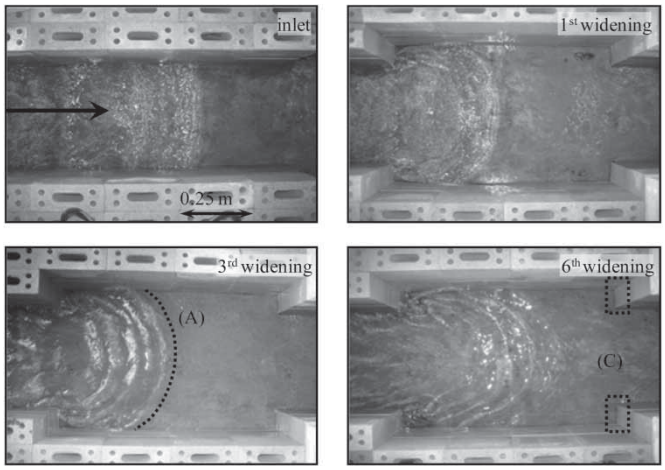

Figure 6 Evolution of positive surge wave from upstream in cavities of widened channel reaches for $L_b = 1.0\,\text{m}$, $L_c = 0.5\,\text{m}$, $\Delta B = 0.1\,\text{m}$, $Q_b = 6.4\,\text{l/s}$, $Q_{total} = 24.9\,\text{l/s}$. (A) Deformation, (C) reflection of surge wave front

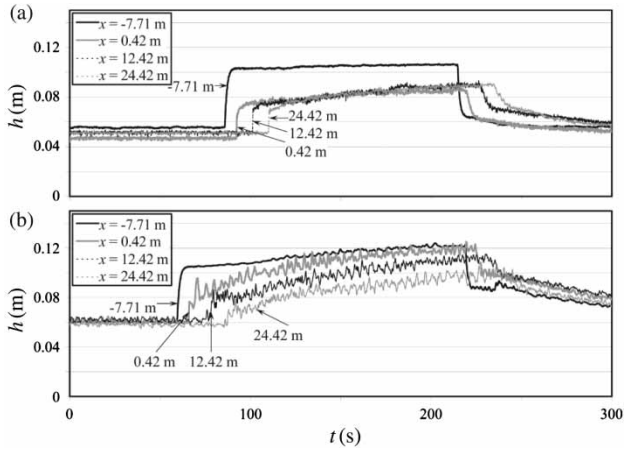

Figure 7 Water-level recordings of positive surge followed by negative surge at four positions along channel in (a) prismatic reference channel, (b) macro-rough channel with rectangular cavities $L_b = 1\,\text{m}$, $L_c = 1\,\text{m}$, $\Delta B = 0.2\,\text{m}$ (configuration 222). $Q_b \cong 11\,\text{l/s}$ and $Q_{total} \cong 28\,\text{l/s}$ for both cases

4.2 *Front wave shape and secondary waves for macro-rough configurations*

In configurations including macro-roughness elements, the surge wave propagation is affected by the storage of water in the cavities and the partial reflection of the surge wave front in the widened channel sections (Fig. 6). The surge wave front and secondary waves are two-dimensional in the prismatic channel but become three-dimensional when entering the cavities, since the streamwise velocities are higher in the extension of the main channel than in the cavities. The combination of all these effects results in an attenuation of the surge wave speed and front height along the macro-rough channel. Furthermore, secondary waves are reduced and or even disappear.

Roughness elements along the macro-rough reach modify the wave front shape and the secondary waves. Compared with the corresponding Runs of the prismatic channel, the following changes were observed in the outlet reach (observation window):

(1) Either the highly-breaking surge wave front for the prismatic configuration changed into a wave front followed by secondary waves for the configuration including macro-roughness elements.
(2) Or the highly-breaking surge wave front (prismatic configuration) changed into a (sudden) rise of the water surface. Secondary waves were no longer present.
(3) Or the non-breaking wave front followed by secondary waves (prismatic configuration) changed into a (sudden) rise of the water surface at the observation window. Secondary waves were no longer present.

The detection of the exact wave front position was difficult in macro-rough configurations due to the irregular water surface. In the prismatic reference configuration, the water surface is quite homogeneous up- and downstream of the surge front, which simplifies the detection of the surge front. E.g. in Fig. 7, the water-level recordings of a positive surge followed by a negative surge along the channel are compared for the prismatic reference channel and a macro-rough bank configuration. At the wave front, different surge conditions were observed for both the prismatic and macro-rough configurations: (1) breaking surge wave front, (2) breaking of first undulation of surge wave followed by secondary waves, also called "Favre waves", (3) non-breaking surge wave front followed by secondary waves and (3) non-breaking surge wave front without detectable secondary undulations.

4.3 *Surge wave front speed*

The absolute wave speed remained practically constant, but reduced as compared with the prismatic reference. For all tested configurations, the reduction of the absolute celerity of positive surges $V_w^+ = U + c^+$ lies between 5% (Runs 141, 241 and 441) and 25% (Runs 114, 214 and 414) compared with the prismatic reference, where U is a representative mean flow velocity of the base-flow and c^+ the wave celerity of the positive surge.

The reduction of wave celerity compared with the prismatic reference is shown in Fig. 8 for the four macro-rough bank Runs 221, 222, 223 and a randomly-generated configuration versus the observed upstream surge Froude number $\mathsf{F_s}$ in the prismatic reference channel defined as

$$\mathsf{F_s} = \frac{(V_w - U_1)}{\sqrt{gh_1}} = \sqrt{\frac{h_2}{2h_1^2}(h_2 + h_1)} \qquad (2)$$

Note from Fig. 8:

- Ratio $V_w^+ / V_{w\ prism}^+$ is nearly constant for a given geometry and thus almost independent of $\mathsf{F_s}$.
- Absolute surge wave celerity reduces (decreasing values of the ratio $V_w^+ / V_{w\ prism}^+$) for increasing ΔB and decreasing L_c.

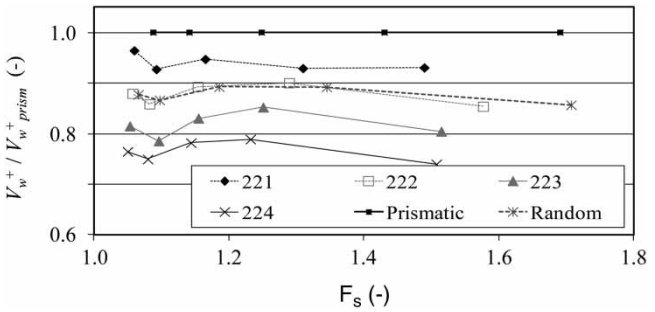

Figure 8 Relative reduction $V_w^+/V_{w\,\text{prism}}^+$ of absolute surge wave celerity of positive surge waves from upstream versus upstream surge Froude number F_s for $L_b = 1$ m, $L_c = 1$ m, with ΔB from 0.1 m (configuration 221) to 0.4 m (configuration 224)

- Higher scattering occurs for $F_s = 1$ because it was difficult to accurately detect the absolute wave celerity of small surge waves in the macro-rough configurations.

4.4 *Effect of macro-roughness on wave celerity*

The relative celerity of the positive surge c^+ results by subtracting the mean flow velocities U_1^+ (condition before the positive surge passage) from the absolute celerity V_w^+ and V_w. For the macro-rough configurations, the mean flow velocities are obtained by the approach of effective channel width as

$$U_1^+ = \frac{\sum_i \Delta x_i \cdot Q_b/(B_{eff} \cdot h_i)}{\sum_i \Delta x_i} \tag{3}$$

where Δx_i = length for which h_i (flow depth measured at i) is representative. For the reference channel and for all reaches between the cavities, B_{eff} is equal to the channel base width B. At the location of the rectangular cavities, the effective width results from flow expansion into the macro-scale depression roughness elements at the banks as

$$B_{eff} = (B + \Delta B)\left(\frac{x_p \Delta B}{L_b}\right) + (B + 2\Delta B)\left(\frac{L_b - x_p \Delta B}{L_b}\right) \tag{4}$$

The flow expands inside the cavity and reattaches at distance $L_1 = x_p \Delta B$ again to the cavity sidewall if the cavity is long enough ($L_b > L_1$). The flow expansion coefficient x_p in Eq. (4) was empirically found from steady flow tests as (Meile *et al.* 2011)

$$x_p = \left(\frac{R_{lim}}{R_m} + x_{p0}\right)\left(\frac{L_b}{\Delta B}\right)^{0.18} \tag{5}$$

with $R_{lim} = 150,000$, $x_{p_0} = 4.5$ and the base channel width-related Reynolds number $R = UR_h/\nu^{-1}$. Comparisons between the observed relative celerity $c = V_w - U$ in the macro-rough channel and the calculated reference celerity based on Eq. (1) are shown in Fig. 9 for 5 Runs and all tested macro-rough configurations. Since the reference values assume frictionless conditions from Eq. (1), it is not surprising that for all Runs and macro-rough

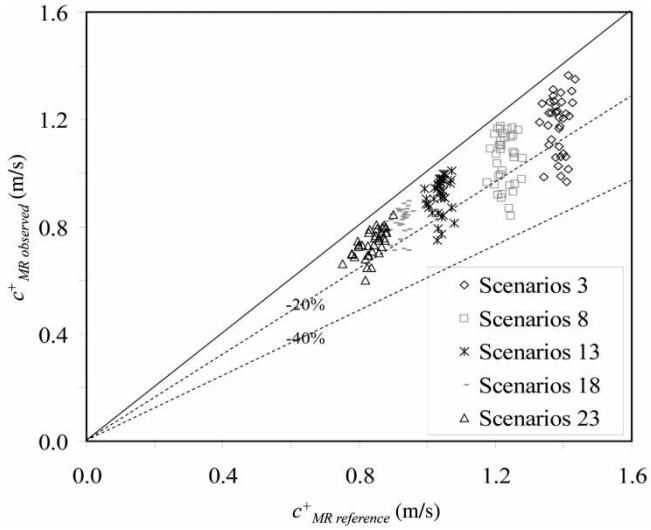

Figure 9 Comparison of observed and from Eq. (1) calculated, reference positive surge wave celerity after subtraction of representative mean flow velocity U_1^+ (Eq. 4) and assuming that bank cavities contribute partially to flow with B_{eff} (Eqs. 6, 7)

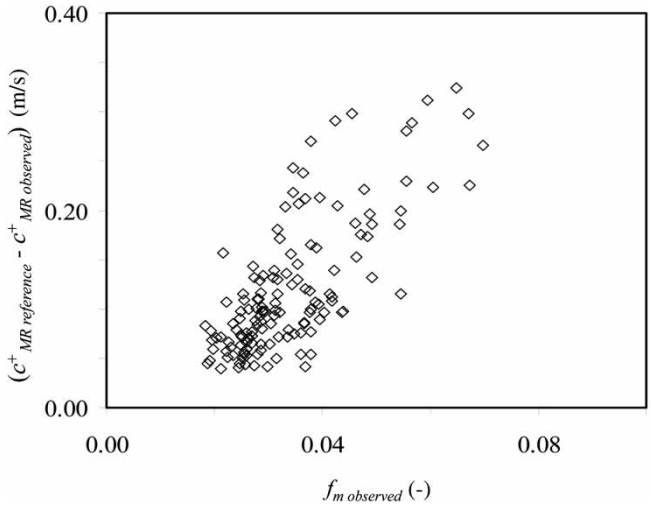

Figure 10 Difference between $c_{MR\,reference}$ and $c_{MR\,observed}$ versus friction coefficient $f_{m\,observed} = f_{prism} + f_{MR}$ relating to Q_b and obtained from steady flow tests

configurations the observed celerities are significantly lower, namely between 5 and 30% for the positive surge waves from upstream (Fig. 9). Thus, the increased flow resistance due to macro-rough banks has a significant effect on the wave celerity.

To underline this statement, the difference between the theoretical, reference celerity $c_{MR\,reference}$ according to Eq. (1) and those observed $c_{MR\,observed}$ are shown in Fig. 10 versus the overall Darcy–Weisbach friction coefficient $f_{m\,observed} = f_{prism} + f_{MR}$ obtained from steady flow conditions (Meile *et al.* 2011). Even if the scatter is high due to the different flow features of the macro-rough configurations, namely square-grooved, reattachment and normal recirculating flow types, a clear trend results related to the dependence between relative wave celerity in the macro-rough configurations and the overall friction coefficient.

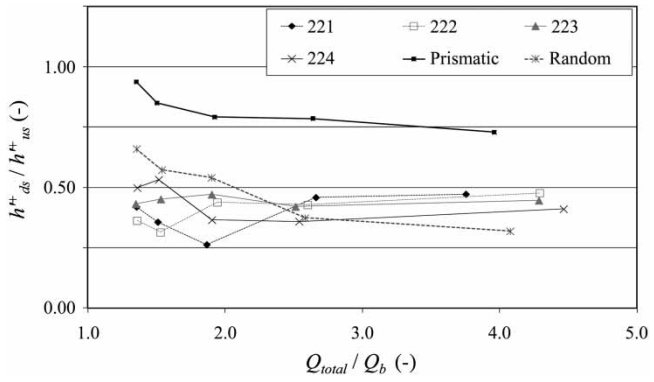

Figure 11 Observed surge wave height ratio between beginning and end of macro-rough reach for positive surge from upstream h'^{+}_{ds}/h'^{+}_{us} versus Q_{total}/Q_b for macro-rough configurations 221–224 and randomly-generated macro-rough configuration

A similar decrease in the front celerity was also observed for dam-break waves affected by friction (Dressler 1954, Whitham 1955, Lauber and Hager 1998a, 1998b, Leal *et al*. 2006).

4.5 *Attenuation of surge wave front height*

The analysis of the measured surge wave front height confirms the dispersive character of surge waves or the attenuation of the surge wave front height. The increased attenuation in the macro-rough bank configurations depends on the macro-rough flow resistance and other phenomena including the partial reflections of the surge wave in the cavities of the depression macro-roughness and the passive cavity retention. An example of the observed surge wave height ratio between the start and the end of the macro-rough reach is given in Fig. 11 versus the surge characteristic Q_{total}/Q_b. Runs 221, 222, 223 and one randomly created are compared with the prismatic reference channel. Along the prismatic channel, the ratio between the up- and downstream heights of the surge wave front h'^{+}_{ds}/h'^{+}_{us} indicates a height decrease in the positive surge wave front $h\prime^{+}$ of 5% for low discharge ratios Q_{total}/Q_b to 25% for high Q_{total}/Q_b. Considering all tested macro-rough configurations, the decrease of h'^{+} is much higher, namely up to 70%.

Meile (2007) described the attenuation of the surge wave front height by empirical relations with a slightly modified approach as presented by Lai *et al*. (2000). The tendency of the effect of the large-scale bank roughness on the front height attenuation was reproduced, but the coefficients of determination of the developed empirical relationships remained moderate due to the high scatter of the data.

5 Conclusions

Systematic experiments of positive and negative surge waves were conducted in prismatic and macro-rough channels. The absolute wave celerity along the macro-rough reach remains practically constant, but reduces when compared with the prismatic reference. Constant values of the positive surge along the channel are explained by Froude numbers relatively close to 0.5. The reduction of the absolute celerity of the surge wave front from upstream lies between 5 and 25% compared with the prismatic reference. The reduction in the absolute surge wave celerity in the macro-rough configurations is attributed to:

(1) Due to a backwater-curve, the flow depths increase and thus the mean flow velocity decreases from down- to upstream along the channel. The absolute surge wave celerity should therefore *a priori* decrease compared with the prismatic reference. However, the decrease in the mean flow velocity is partially compensated for by the increase in the relative celerity due to the higher water levels.
(2) An additional decrease in the mean flow velocity results from the partial expansion of the flow in the widened channel reaches.
(3) The surge wave front height is attenuated along the macro-rough reach, resulting in attenuation of the celerity.

It is not obvious to distinguish the various effects. However, assuming a conceptual flow expansion model, the difference between the observed and the theoretical celerity calculated based on the flow depths before and after the surge wave front confirms the important effect of flow resistance. The friction coefficients relate to steady flow before surge wave arrival. The dispersive character of surge waves was experimentally observed. The surge front height decreases in particular in the macro-rough configurations. Due to the high scatter of the experimental data, the attenuation of the surge wave front height is difficult to describe with an empirical formula.

Acknowledgement

The Swiss Federal Office for the Environment supported this research project.

Notation

B = channel base width (m)
ΔB = lateral cavity depth (m)
B_{eff} = representative width for mean flow velocity (m)
C = Chézy coefficient ($m^{0.5}/s$)
c = relative celerity (m/s)
f = Darcy–Weisbach friction coefficient (–)
F_s = surge Froude number (–)
g = gravity constant (m/s^2)
h = flow depth (m)
$h\prime$ = height of surge wave front (m)
k_s = equivalent sand roughness height (m)
L_b = length of cavity (m)
L_c = cavity spacing (m)

P = wetted perimeter (m)
Q = discharge (m^3/s)
R = Reynolds number relative to B (–)
R_h = hydraulic radius (m)
R_{lim}; x_{p_0} = constant of empirical flow expansion formula (–)
t = time (s)
U = mean flow velocity (m/s)
V_w = absolute celerity of surge wave front (m/s)
X = dimensionless distance (–)
x_p = flow expansion coefficient (–)
x_0 = reference location along x-axis (m)
x_i = positions i of ultrasonic-probes (m)
Δx_i = representative length for flow depths measured at sensor I(m)

Subscripts

0 = channel bottom
1, 2 = sections before and after surge wave front
b = base-flow
MR = macro-roughness
m = composite section; overall flow resistance
observed = observed celerity
prism = flow resistance of prismatic reference channel
reference = calculated reference celerity according to Eq. (1)
total = total discharge
us, ds = up- and downstream section
w = wall

Superscript

+ = positive surge from upstream

References

Bazin, H. (1865). *Recherches expérimentales relatives aux remous et à la propagation des ondes* [Experimental researches relative to backwater and wave propagation]. Dunod, Paris (in French).

Benet, F., Cunge, J.A. (1971). Analysis of experiments on secondary undulations caused by surge waves in trapezoidal channels. *J. Hydraulic Res.* 9(1), 11–33.

Chow, V.T. (1959). *Open-channel hydraulics*. McGraw-Hill, New York.

Chung, W., Kang, Y. (2006). Classifying river waves by the Saint-Venant equations decoupled in the Laplacian frequency domain. *J. Hydraulic Eng.* 132(7), 666–680.

Dressler, R.F. (1954). Comparison of theories and experiments for the hydraulic dambreak wave. *Int. Assoc. Sci. Hydrology* 3(38), 319–328.

Faure, J., Nahas, N. (1961). Etude numérique et expérimental d'intumescences à forte courbure du front [Numerical and experimental study of travelling surges with strong front curvature]. *La Houille Blanche* 16(5), 579–587 (in French).

Favre, H. (1935). *Etude théorique et expérimentale des ondes de translation dans les canaux découverts* [Theoretical and experimental study of travelling surges in open channels]. Dunod, Paris (in French).

Graf, W.H., Altinakar, M.S. (1996). *Hydraulique fluviale, écoulement non permanent et phénomènes de transport* [Fluvial hydraulics, unsteady flows and transport phenomena]. PPUR, Lausanne, Switzerland (in French).

Henderson, F.M. (1966). *Open channel flow*. Macmillan, New York.

Lai, C.-J., Liu, C.L., Lin, Y.-Z. (2000). Experiments on flood-wave propagation in compound channel. *J. Hydraulic Eng.* 126(7), 492–501.

Lauber, G., Hager, W.H. (1998a). Experiments to dambreak wave: Horizontal channel. *J. Hydraulic Res.* 36(3), 291–307.

Lauber, G., Hager, W.H. (1998b). Experiments to dambreak wave: Sloping channel. *J. Hydraulic Res.* 36(5), 761–773.

Leal, J.G.A.B., Ferreira, R.M.L., Cardoso, A.H. (2006). Dam-break wave front celerity. *J. Hydraulic Eng.* 132(1), 69–76.

Meile, T. (2007). Influence of macro-roughness of walls on steady and unsteady flow in a channel. *PhD thesis*, Ecole Polytechnique Fédérale de Lausanne and Communication No. 36, Laboratory of Hydraulic Constructions, A. Schleiss, ed., Lausanne, Switzerland.

Meile, T., Boillat, J.-L., Schleiss, A.J. (2008). Improvement of acoustic Doppler velocimetry in steady and unsteady turbulent open-channel flows by means of seeding with hydrogen bubbles. *Flow Meas. Instrument.* 19(3/4), 215–221.

Meile, T., Boillat, J.-L., Schleiss, A.J. (2010). Hydropeaking indicators for characterization of the Upper-Rhone River in Switzerland. *Aquatic Sciences* 73(1), 171–182.

Meile, T., Boillat, J.-L., Schleiss, A.J. (2011). Flow resistance due to large-scale bank roughness in a channel. *J. Hydraulic Eng.* 137(12), 1588–1597.

Morris, H.M. (1955). Flow in rough conduits. *Trans. ASCE* 120(1), 373–410.

Ponce, V. M., Li, R. M., Simons, D. B. (1978). Applicability of kinematic and diffusive models. *Journal of Hydraulic Division* - ASCE, 104(3), 353-360.

Schoklitsch, A. (1917). Über Dammbruchwellen [On dam-break waves]. *Sitzungsberichte Kaiserliche Akademie der Wissenschaften Wien* 126(10), 1489–1514 (in German).

Soares-Frazão, S., Zech, Y. (2002). Undular bores and secondary waves: Experiments and hybrid finite – volume modelling. *J. Hydraulic Res.* 40(1), 33–43.

Treske, A. (1994). Undular bores (Favre-waves) in open channels: Experimental studies. *J. Hydraulic Res.* 32(3), 355–370.

Ünsal, I. (1983). Propagation of dam-break waves in channels of varying section. Proc. *20th IAHR Congress*, Moscow, 539–545.

Whitham, G.B. (1955). The effects of hydraulic resistance in the dam-break problem. Proc. *R. Soc. A* 227(1170), 399–407.

Zairov, K.I., Listrovoy, P.P. (1983). Experimental investigation of the positive traveling surges fore-part observed in canals. Proc. *20th IAHR Congress*, Moscow, 210–218.